Mitigating the autogenous shrinkage of alkali-activated slag by metakaolin

Li, Zhenming; Nedeljković, Marija; Chen, Boyu; Ye, Guang

DOI
10.1016/j.cemconres.2019.04.016

Publication date
2019

Document Version
Accepted author manuscript

Published in
Cement and Concrete Research

Mitigating the autogenous shrinkage of alkali-activated slag by metakaolin

Zhenming Li[a], Marija Nedeljković[a], Boyu Chen[a], Guang Ye[a,b]

[a]Department of Materials and Environment (Microlab), Faculty of Civil Engineering and Geoscience, Delft University of Technology, Delft, the Netherlands
[b]Magnel Laboratory for Concrete Research, Department of Structural Engineering, Ghent University, Ghent, Belgium

Abstract

This study investigates the effectiveness of metakaolin (MK) in mitigating the autogenous shrinkage of alkali-activated slag (AAS). It is found that the autogenous shrinkage of AAS paste can be reduced by 40% and 50% when replacing 10% and 20% slag with MK, respectively. By providing additional Si and Al, and decreasing the pH of the pore solution, the incorporation of MK retards the formation of aluminium-modified calcium silicate hydrate gels, the main reaction products in the studied pastes. The chemical shrinkage and pore refinement are consequently mitigated, resulting in a substantial reduction in the pore pressure. Meanwhile, the elastic modulus of AAS paste is only slightly influenced after MK addition. As a result, the autogenous shrinkage of AAS is significantly mitigated by incorporating MK. In addition, the introduction of MK would extend the setting time, slightly decrease the compressive strength, but greatly increase the flexural strength of AAS.

Keywords:

Slag, shrinkage, mitigation, metakaolin, mechanical properties

1. Introduction

Alkali-activated slag (AAS), as a clinker-free alternative to ordinary Portland cement (OPC), has been studied for more than 100 years [1–3]. Although AAS exhibits high mechanical strength, high resistance to chemical attack and good thermal performance [4–6], the high autogenous shrinkage of AAS hampers its wider application in construction industry [7,8].

Intensive research has been conducted to investigate the autogenous shrinkage magnitudes, mechanisms and mitigating strategies of AAS [9–16]. Cured in sealed condition, AAS was found to shrink 10 times as much as OPC [16]. The high negative pore pressure generated in the fine pores of AAS during self-desiccation was commonly assumed to be the main driving force for the large autogenous shrinkage [11,14,17–19]. Moreover, AAS tends to deform more than OPC-based pastes even under the same pressure due to the high viscoelasticity of the aluminium-modified calcium silicate hydrate (CASH) gels [14,20].

Currently, four types of strategies have been investigated by researchers to mitigate the autogenous shrinkage of AAS systems.

- Internal curing, by either lightweight aggregates (LWA) such as pumice and expanded clay or superabsorbent polymers (SAP) [13,21–23]. By introducing LWA or SAP into the system, liquid reservoirs are created and extra water or alkali solution would be provided during hydration to compensate for the liquid consumption. In this way, the pore pressure induced by self-desiccation will be mitigated. According to previous research

[13,22,23], the main drawback of this method is the reduction of the early age compressive strength of AAS systems, especially for the systems with LWA.

- Shrinkage reducing admixtures (SRA) or expansive agents. A SRA for OPC-based system was found to effectively reduce the autogenous shrinkage of AAS according to Ballekere et al.[21]. However, it is important to note that not all of the admixtures or agents that are widely used in OPC systems work effectively in alkali-activated systems [24–26]. For example, the use of CaO as an expansive agent was found to increase the shrinkage of AAS, which was probably due to the refinement of the pore structure with incorporation of CaO [15]. Another example is gypsum, which can initiate the formation of expansive phases at the early age to reduce the shrinkage of AAS, but this early-age expansion was insufficient to compensate the subsequent long-term shrinkage [15]. Hence, suitable SRA for alkali-activated materials need to be identified.
- Elevated temperature curing. Curing the samples at temperature from 60 °C to 80 °C was reported to be helpful to reduce the drying shrinkage of AAS due to the reduction in the viscoplastic/viscoelastic compliance of CASH gels [15,27,28]. In this case, elevated temperature curing may also be effective in mitigating the autogenous shrinkage of AAS since the since the autogenous shrinkage is also critically influenced by the deformability of the gels [14]. However, the high requirement on the facilities to provide elevated temperature, as the inherent disadvantage of this strategy, makes it less suitable for cast-in-situ concrete compared with precast concrete.
- Incorporation of other precursors. Activation of slag with other precursors can counterbalance the disadvantages shown by pure slag-based systems. For example, the incorporation of fly ash, another commonly utilized industrial by-product, has been intensively reported to be effective in reducing the autogenous shrinkage of AAS [16,19,29–31]. It is found that substitution of 30% and 50% slag by fly ash can lead to 15% and 40% reduction of the autogenous shrinkage, respectively [16]. However, the reduction was mainly due to the filler's effect of fly ash to reduce the "real" binder content in the system, which only worked when a large amount of fly ash was incorporated. This method is, therefore, less attractive in the areas where fly ash is not largely available.

Compared with fly ash, metakaolin (MK) is more reactive at ambient temperature upon alkali activation. Therefore, it may have advantages over fly ash in terms of mitigating autogenous shrinkage and improving other properties of AAS. Regarding alkali-activated slag-MK binary system, many studies have been carried out to investigate its microstructural characteristics and engineering properties [32–35]. Coexistence of CASH gel and sodium aluminosilicate hydrate (NASH) gel was found when the blends were cured at elevated temperature [32–34]. At ambient temperature, the reaction products were found to be dominated by CASH type gels, part of which can be C(N)ASH where Ca^{2+} was exchanged with Na^{+}, but the 2D gel structure remained [36,37]. The addition of MK can improve the workability [38], postpone the final setting [38], enhance the flexural strength [39], and decrease the chloride permeability of AAS [39]. Moreover, MK also helps to mitigate the alkali-silica reaction and enhance the high-temperature stability of AAS mortar [40]. A disadvantage induced by MK addition is the increase of the carbonation rate of AAS [41]. MK addition also leads to a potential reduction in the compressive strength, but that is only to a limited extent, especially when the content of MK is low (e.g. 10% - 20%) [39,42]. Given the improvements of the properties of AAS by addition of MK, it would be very interesting to know its potential to mitigate the autogenous shrinkage of AAS. However, no studies have been published

related to this aspect yet, to the best knowledge of authors.

The aim of this paper, therefore, is to investigate the effectiveness of MK in mitigating the autogenous shrinkage of AAS, and to study the mechanisms behind. For this purpose, the development of autogenous shrinkage, reaction products, hydration heat, ions concentrations in the pore solutions, pore structure, chemical shrinkage and internal relative humidity (RH) of AAS pastes with and without MK are comprehensively investigated. Mechanical properties of the studied pastes are also measured. The finding that the autogenous shrinkage of AAS can be effectively mitigated by a small amount of MK, which is cheap and widely available, is valuable in widening the commercial acceptance of slag based alkali-activated materials as binder materials.

2. Methodological approach

2.1 General framework of the study

In the first part of this paper, the autogenous shrinkage of AAS pastes with and without MK is presented.

In the second part, the mechanism of the effectiveness of MK in mitigating the autogenous shrinkage of AAS was explored. The framework of this part is shown in Fig.1. Autogenous shrinkage of AAS can be considered as a result of the competition between the driving force - pore pressure and the resistance – bulk modulus of the AAS skeleton [17,21]. These two parameters are both dependent on the microstructure development of the paste. Therefore, as the first step of this part, the reaction products, reaction kinetics and pore structures of AAS with and without MK were characterized with the help of X-ray diffraction (XRD), Fourier transform infrared spectroscopy (FTIR), calorimetry, inductively coupled plasma optical emission spectrometry (ICP- OES) and nitrogen absorption. As the second step, the evolution of chemical shrinkage was measured and clarified. The internal RH was measured as the input for the calculation of the pore pressure. Finally, the elastic modulus of the samples was tested to indicate the stiffness of the mixtures.

In the third part, the compressive and flexural strength of the pastes were measured for a better understanding of the influence of MK addition on the mechanical properties of AAS paste.

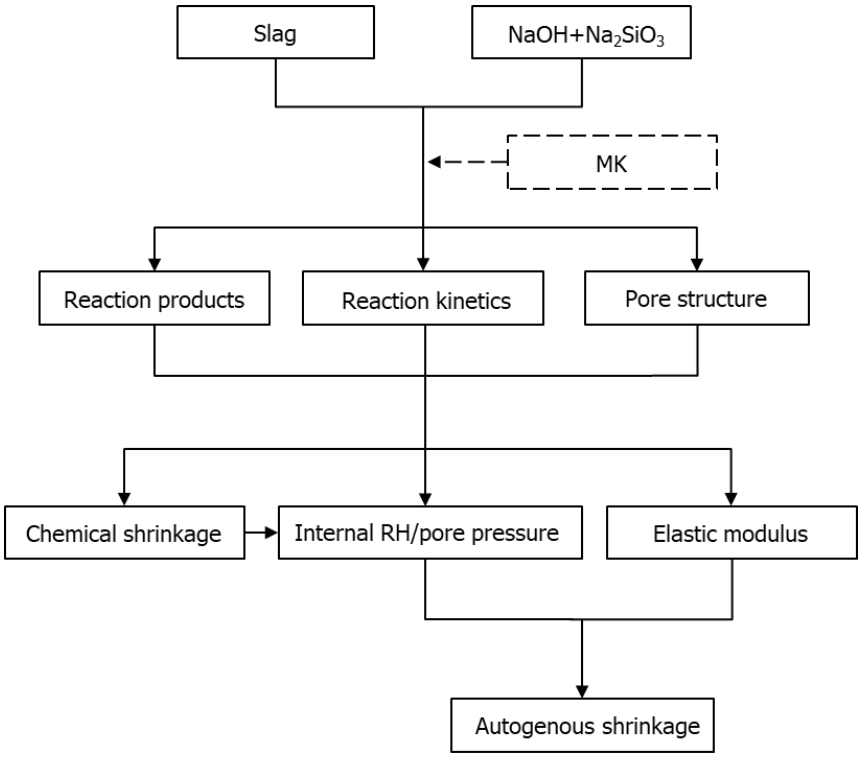

Fig.1. Approach to study the autogenous shrinkage-mitigating mechanisms of MK addition.

2.2 Materials and sample preparation

The primary raw material used in this study was granulated blast-furnace slag (BFS) supplied by ORCEM (the Netherlands). The chemical composition of BFS was determined by X-ray fluorescence (XRF) (as shown in Table 1). The particle size, as determined by laser diffraction analyzer, ranges from 0.1 to 50 µm, with a d_{50} of 18.3 µm. Metakaolin (MK) was supplied by Argeco (France). The particle size of the MK is between 0.15 and 142 µm, with a d_{50} of 69.4 µm.

Table 1

Chemical compositions of BFS and MK measured by XRF.

Precursor	**Component (mass% as oxide)**									
	SiO_2	Al_2O_3	CaO	MgO	Fe_2O_3	SO_3	K_2O	TiO_2	Other	LOI
BFS	31.77	13.25	40.50	9.27	0.52	1.49	0.34	0.97	0.21	1.31
MK	55.14	38.43	0.55	-	2.6	-	0.17	1.12	0.14	1.85

LOI= Loss on ignition

The alkaline activator was prepared by mixing anhydrous pellets of sodium hydroxide with deionized water and commercial sodium silicate solution (27.5 wt% SiO_2, 8.25 wt% Na_2O). A relatively high alkalinity environment (9.3% Na_2O by mass of BFS+MK) was created to attain a dense microstructure and good mechanical properties according to [39]. The paste mix design is shown in Table 2. All the samples were cured in sealed condition at 20° C before tested.

Table 2

Mixture proportions of AAS pastes with and without MK.

Mixture	BFS (g)	MK (g)	SiO_2 (mol)	Na_2O (mol)	H_2O (g)
1.0BFS	1000	-	1.146	1.5	420
0.9BFS0.1MK	900	100	1.146	1.5	420
0.8BFS0.2MK	800	200	1.146	1.5	420

2.3 Methods

2.3.1 Autogenous shrinkage measurement

The autogenous shrinkage of the pastes was measured by corrugated tube method [43], in which three sealed corrugated tubes of 420 mm (Ø28.5 mm) were tested for each mixture. After mixing, the fresh paste was carefully cast into the corrugated tubes and sealed by plugs. The specimens and instrument were immersed in a box with glycol. The temperature of the glycol was regulated at 20 ± 0.1 °C with cryostat. The autogenous shrinkage of specimens was recorded every 5 min from final setting time to 7 days. In all tests, the autogenous shrinkage of parallel samples had a similar trend with a deviation as small as 50 μm/m. The results are presented as the average value of three replicates for each mixture.

2.3.2 Characterization of the paste

XRD measurement was conducted to examine the crystalline phases in the samples, with a Philips PW 1830 powder X-ray diffractometer, with Cu Kα (1.5406 Å) radiation, tube setting of 40 kV and 40 mA, a step size of 0.030° and a 2θ range of 5–70°.

FTIR measurement was performed with a TM 100 Optical ATR-FTIR spectrometer over the wavelength range of 600 to 4000 cm^{-1} and a resolution of 4 cm^{-1}.

The TAM-Air-314 isothermal conduction calorimeter was used to measure the heat flow and cumulative heat of the mixtures. Calibration was done at 20 °C before measurements for a period of 120 h. During the experiment, the measuring cells within the calorimeter were kept at 20±0.1 °C. About 5 g of pre-mixed fresh pastes were poured into the glass vials with internal diameter of 24.5 mm. The vials were next sealed and placed in the calorimeter. The whole procedure lasted approximately 15 min from the start of mixing. The data was recorded every 1 min till 5 days. Hydration heat data are presented starting from 0.5 h after mixing, when the initial temperature rise due to external mixing and to handling of the samples had equilibrated. The calorimetry results were normalized by gram of precursor (slag and MK) in the mixture.

Initial and final setting times of the mixtures were determined according to Vicat needle method [44].

ICP-OES was conducted with Optima 5300 DV to measure the concentrations of Na, Ca, Si and Al in the pore solutions extracted from the pastes at 1 day and 7 days of curing. Titration

method with 0.1M HCl solution was used to measure the concentration of OH^- in the pore solutions. Three replicates were tested and the average results are presented.

Due to the fine pore structure of AAS, nitrogen adsorption method instead of mercury intrusion porosimetry was utilized to characterize the pore size distributions of the pastes [45]. The test was conducted on a Micrometrics Gemini VII 2390 V1.03 with a relative pressure ranging from 0.05 to 0.998. Based on the nitrogen adsorption data, Barrett-Joyner-Halenda (BJH) model was used to derive the pore size distribution curve [46].

2.3.3 Chemical shrinkage and internal RH measurement

The chemical shrinkage of the pastes was measured according to the gravimetry method. The detailed procedure was described elsewhere [47]. The average chemical shrinkage of three replicates is presented for each mixture.

The internal RH of the bulk pastes and the pore solutions extracted from the pastes were measured. The internal RH of the pastes cured for 1 day and 7 days was monitored by Rotronic hygroscopic DT station equipped with HC2-AW measuring cells [48]. The paste samples were cut into thin slices (< 7 mm), which were then put into two plastic containers in the measuring chambers. Samples and atmosphere equilibrated in 3-5 hours. Before the measurements, RH probes were calibrated using standard saturated salt solutions with constant RH in the range of 65-95%. The RH of the pore solution (RH_S) was measured in the same way as it was measured for the bulk paste. The deviation of test results was less than 0.5%. Therefore, the average values of three parallel specimens for each sample is presented.

With the measured RH of the paste and the pore solution, the RH due to the curvature effects of the menisci can be calculated by Eq. (1) [49].

$$RH_K = RH/RH_S \quad (1)$$

where RH is the RH of the paste, RH_S is the RH of the pore solution caused by dissolved salts and RH_K is due to the curvature effects of the menisci at the gas-liquid interfaces.

When RH_K is known, the corresponding pore pressures σ (MPa) within the paste can be calculated by Kelvin equation (Eq. (2)) and Laplace equation (Eq. (3)):

$$r = \frac{2\gamma V_w}{\ln(RH_K)RT} \quad (2)$$

$$\sigma = -\frac{2\gamma}{r} \quad (3)$$

where r (m) is the radius of the menisci; γ (N/m) is the surface tension of the pore solution; V_w is the molar volume of the pore solution (m^3/mol); R (J/(mol·K)) is the universal gas constant; T is the temperature expressed in the absolute scale.

By combining Eq. (2) and Eq. (3), the pore pressure within the specimen is obtained:

$$\sigma = -\frac{\ln(RH_K)RT}{V_w} \quad (4)$$

To calculate the pore pressure, the value of V_w can be taken as the one for pure water, i.e., 18.02×10^{-6} m^3/mol according to Lura [50], who reported that the ions has little influence on V_w. The value of R is 8.314 J/(mol·K) and T =293.15 K.

2.3.4 Elastic modulus measurement

The quasi-static elastic modulus of the pastes was measured on 40 × 40 × 160 mm^3 prisms at the age of 1 day and 7 days. The loading was provided by a hydraulic actuator with the maximum load of 100 kN. The strain was measured by four transducers (LVDTs) on each side of the sample. The loading consisted of four cycles with the load ranges from 5% to 30% of the compressive strength and only the stress and strain obtained from the latter three cycles were utilized to calculate the mean elastic modulus. The loading and unloading were in displacement control and the rate was 0.004 mm/second (around 0.6 MPa/second) [51]. Three specimens were tested for each mixture at each age.

2.3.5 Strength measurement

Flexural strength and compressive strength of the pastes were tested in accordance with NEN-196-1 at the curing ages 1 day, 7 days and 28 days [52]. The flexural strength was measured with three-point bending test on 40 × 40 × 160 mm^3 prisms. The compressive strength was carried out on halves of the prism broken during the flexural strength test. Three and six replicates were tested for flexural strength and compressive strength, respectively.

3. Results

3.1 Autogenous shrinkage

As shown in Fig. 2, the plain AAS paste shrinks rapidly after final setting, reaching around 5000 μ strain at 1 day and around 6900 μ strain at 1 week. This magnitude of autogenous shrinkage is more than three times higher than the common autogenous shrinkage of OPC based pastes, which normally show an autogenous shrinkage of less than 2000 μ strain in the first week, except for those prepared at extremely low water/cement ratios (e.g. 0.2) [16,50,53,54]. The large autogenous shrinkage exhibited by 1.0BFS is consistent with the values reported in literature [9,16]. When 10% slag is substituted by MK, the autogenous shrinkage is reduced by 44% at 1 day and 38% at 7 days. A larger content of MK to 20% leads to further reduction in autogenous shrinkage to more than 60% at 1 day and around 50% at 7 days.

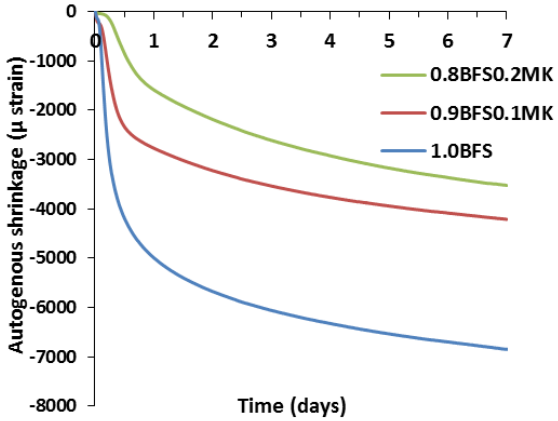

Fig. 2. Autogenous shrinkage of AAS pastes with and without MK.

3.2 Characterization results

3.2.1 XRD analysis

The XRD diffractograms of precursors and pastes are shown in Fig. 3. The XRD pattern of BFS presents a hump around 29° due to the presence of amorphous phase. The plain AAS paste is mainly amorphous. Apart from the background hump related to the unreacted slag, additional diffraction peaks at 29° and 49.8° (marked by the dashed lines) can be observed in the curves of 1.0BFS, which can be attributed to the formation of CASH type gels [55]. These signals become less evident in the specimens with MK incorporation. The crystalline phase identified in the spectra of 0.9BFS0.1MK and 0.8BFS0.2MK is quartz (SiO_2, pdf 01-083-0539) originated from the raw MK. With the increase of curing time, the small hump for CASH gels become more intensive by reference to the intensity for quartz peaks, indicating the formation of larger amounts of amorphous reaction products. The intensities of the humps representing CASH gels in the XRD spectra of 0.9BFS0.1MK and 0.8BFS0.2MK are smaller than that of 1.0BFS at both 1 day and 7 days. This suggests that the amount of CASH gels formed in the first week probably decrease with the increasing content of MK.

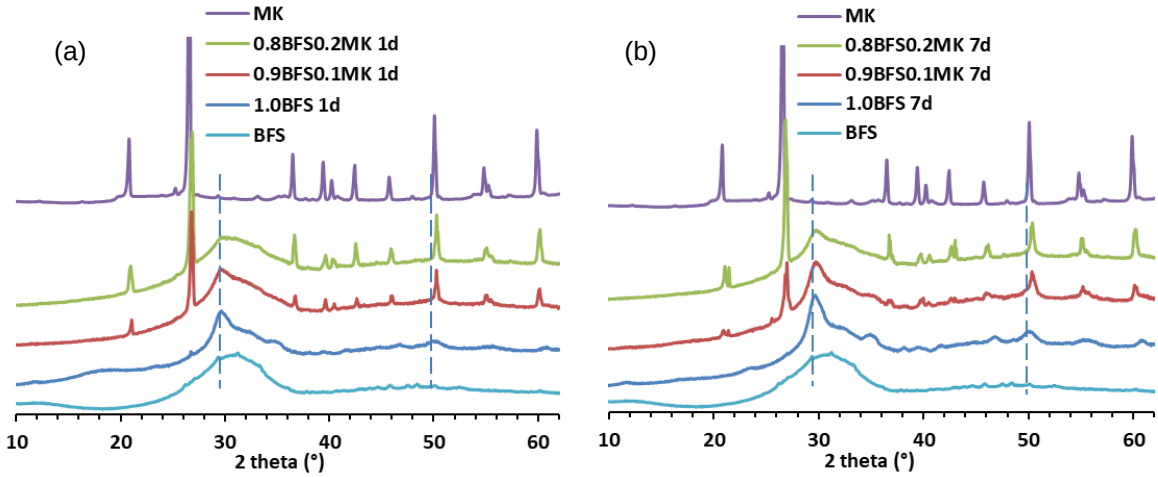

Fig. 3. XRD patterns of precursors (BFS and MK) and pastes cured for (a) 1 day and (b) 7 days.

3.2.2 FTIR analysis

The main bands of the FTIR spectra are all near 942 cm^{-1} (Fig. 4), which is associated with the asymmetrical stretching vibrations of Si–O bonds generated by Q^2 units [37,56,57]. The bands located at around 895 cm^{-1} and 660 cm^{-1} can be assigned to the deformational vibrations of Si-O-Si or Si-O-Al [37,56]. The band at around 815 cm^{-1} is typical for Si–O (Q1) symmetric stretching vibrations [56]. In fact, the signals at 895 cm^{-1}, 815 cm^{-1}, and 660 cm^{-1} are visible in all spectra, and their intensities decrease with increasing content of MK. These results indicate that the dominant reaction product in AAS remains as CASH gel, but the amount of this gel decreases when more MK is introduced to the system, which confirmed the observation in XRD. This finding is also in line with the previous studies on alkali-activated BFS/MK blends [36].

The spectra of 0.9BFS0.1MK and 0.8BFS0.2MK cured for 1 day show also small shoulders in the region from 1050 cm^{-1} to 1075 cm^{-1}, which can be attributed to the asymmetric stretching vibrations of Si-O-T (T: Si or Al) in three-dimensionally structured NASH type gels

[26,37,58,59]. However, these signals become nearly invisible after curing for 7 days (as can be seen in Fig. 4 (b)), revealing that the NASH gels formed at very early age disappeared in prolonged curing time.

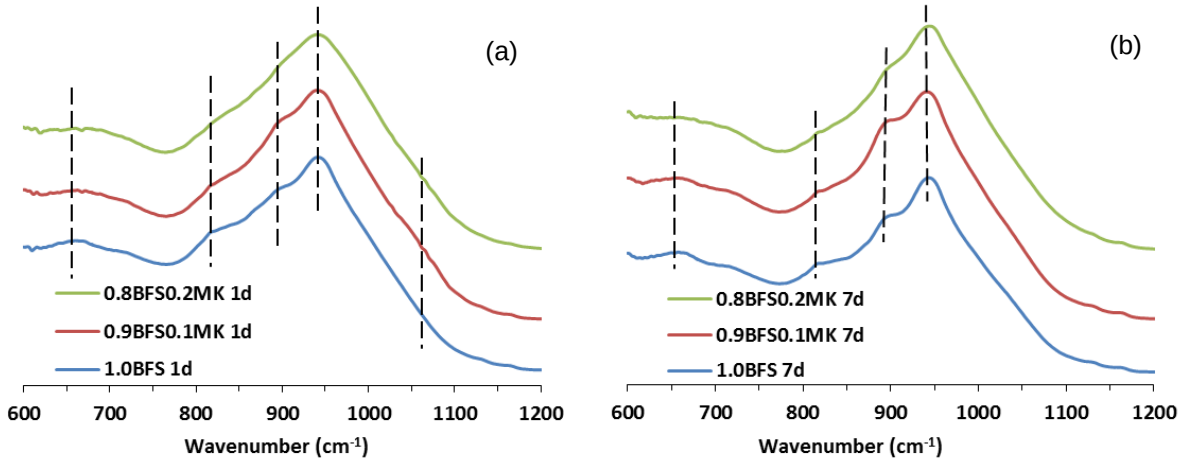

Fig. 4. FTIR spectra of AAS pastes with and without MK cured for (a) 1 day and (b) 7 days.

3.2.3 Isothermal heat release and setting time

As shown in Fig. 5 (a), the heat flows curves of the mixtures appear to follow a similar tendency as described in previous research on slag based alkali activated materials [60–63]. The initial peak (as amplified in the panel in Fig. 5 (a)) detected during the first few minutes of reaction may correlate to wetting and initial dissolution of the precursors. The main peak identified at the later stage of reaction represents the reactions among the dissolved species, corresponding to the acceleration period. The main peak for 1.0BFS appears immediately after the initial peak. Replacing 10% slag with MK delays the appearance of the acceleration period and decreases the intensity of the main peak, suggesting that the formation of the majority of reaction products slows down due to the addition of MK. This effect becomes more significant when 20% MK is added into the system. These results are in agreements with the XRD and FTIR results where 0.9BFS0.1MK 1d and 0.8BFS0.2MK 1d show less intensive and less sharp main band compared to 1.0BFS 1d.

The cumulative heat of the pastes is shown in Fig. 5 (b). The heats released by the three mixtures are similar during the first 3 hours. Although the heat flow of 0.9BFS0.1MK is lower than that of 1.0BFS during the acceleration period, the two mixtures release similar amount of total heat at 120 hours. For 0.8BFS0.2MK, the total heat release is lower than the other two mixtures in the whole period studied except the first 3 hours. It can be noticed that the heat releases of the three mixtures are lower than the common heat release of OPC pastes, which is normally more than 200 J/g in ambient temperature within 5 days [64]. This finding is in line with the results reported by Krizan and Zivanovic [65].

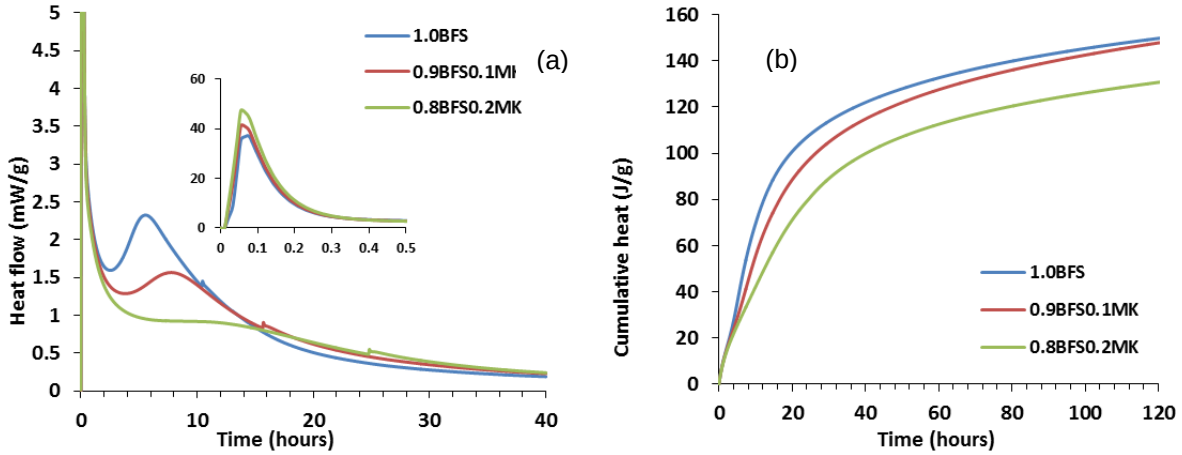

Fig. 5. Heat release of AAS pastes with and without MK (the initial peak is amplified and inset at the top-right corner).

The Vicat setting time of the three mixtures is presented in Table 3. When 10% of MK is incorporated, the initial setting time and final setting time of AAS are increased by 7 mins and 22 mins, respectively. Increasing the content of MK from 10% to 20% results in longer setting time, but the effect is not pronounced.

Table 3

Setting times of AAS pastes with and without MK measured by Vicat method.

Mixtures	Initial setting (min)	Final setting (min)
1.0BFS	33	59
0.9BFS0.1MK	40	82
0.8BFS0.2MK	45	85

3.2.4 Pore solution compositions

The elemental concentrations of Ca, Na, Si and Al and the ions concentration of OH^- are shown in Fig. 6. It can be seen from Fig. 6 (a) that the concentrations of Na^+ and OH^- are lower in the pore solutions of 0.9BFS0.1MK and 0.8BFS0.2MK than in 1.0BFS at both 1 day and 7 days. This is probably due to the consumption of these ions during the dissolution of MK and the formation of initial NASH gels [66]. Fig. 6 (b) shows that the concentration of Ca in the pore solutions decreases with the increase of MK content. The much lower Ca concentrations in MK-containing samples indicate either retarded dissolution of slag or faster precipitation of the ions to form CASH gels. The latter one seems not to be the case here according to the longer induction periods of 0.9BFS0.1MK and 0.8BFS0.2MK shown in Fig. 5. Therefore, it's highly probable that the dissolution of slag is prohibited when MK is present. The retarded dissolution of slag may be attributed to the lower concentration of Na^+ and OH^- in 0.9BFS0.1MK and 0.8BFS0.2MK as shown in Fig. 6 (a). Besides, the dissolution of MK releases more Si and Al to the pore solution especially at early age, as shown in Fig. 6 (c).

At the age of 7 days, the divergence of the concentrations of Ca, Si and Al in different

mixtures become less distinct. This is in line with the FTIR results which show that similar final reaction products (CASH type gels) are formed in the three systems at the age of 7 days.

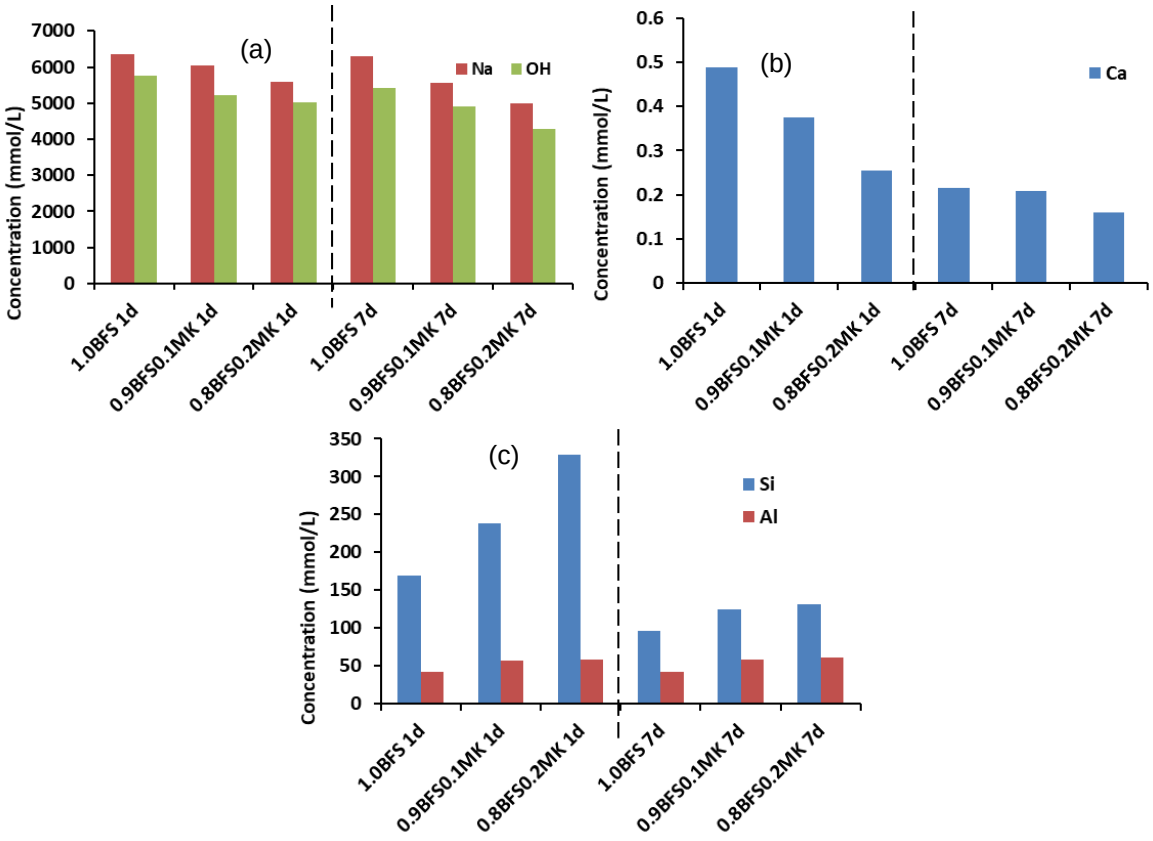

Fig. 6. Concentrations of (a) Na and OH, (b) Ca, (c) Si and Al of the pore solutions of AAS pastes with and without MK.

3.2.5 Pore size distribution

Fig. 7 shows the pore size distribution and differential curves, derived from nitrogen adsorption, for AAS paste with and without MK at the curing ages of 1 day and 7 days. The pores detected by N_2 adsorption are of sizes between 2 nm and 250 nm.

It can be observed that a large part of the pores in the mixtures are small pores within the range of 2 nm-10 nm, corresponding to gel pores. The differential curves of the pore size distribution show one main peak, although the curves for 0.9BFS0.1MK and 0.8BFS0.2MK also show some small peaks at the pore diameter between 30 nm to 90 nm, which are in the range of capillary pores. As curing age increases, the main peaks of the three mixtures all shift to smaller pore diameters, and the amplitudes decrease, indicating the formation of denser structures. By comparing the pore volumes in 1.0BFS, 0.9BFS0.1MK and 0.8BFS0.2MK, it can be seen that the introduction of MK induces a coarser pore structure of the paste in the whole period studied.

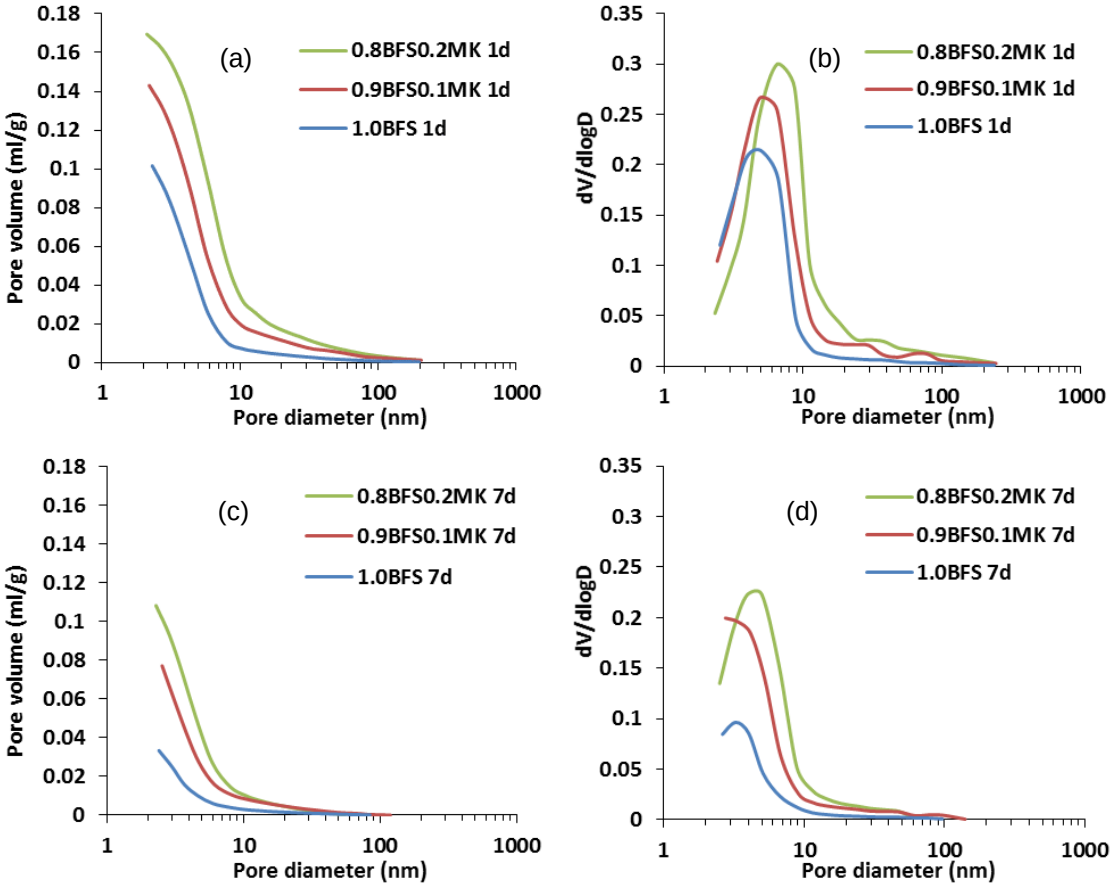

Fig. 7. Pore size distribution and differential curves, derived from nitrogen adsorption, for AAS pastes with and without MK cured for 1 day (a,b) and 7 days (c,d).

3.3 Chemical shrinkage

Fig. 8 shows that the chemical shrinkage of the mixtures can be divided into two stages. The position of the turning point between the two stages is found to correspond well with the moment when the heat release rate of the mixture reaches the maximum, as shown in Fig. 9, where the chemical shrinkage curves and the heat flow curves are plotted together. The first stage of chemical shrinkage is due to the fast dissolution of the precursor while the second stage represents the formation of reaction products.

In the first stage, the mixtures with a higher content of MK show higher chemical shrinkage which may be attributed to the fast dissolution of MK [47]. After the turning point, the chemical shrinkage of 1.0BFS surpasses the other two mixtures, which is probably due to the retarded formation of reaction products in 0.9BFS0.1MK and 0.8BFS0.2MK, as shown by Fig. 3 - Fig. 5. Similarly, the chemical shrinkage of 0.9BFS0.1MK develops faster than that of 0.8BFS0.2MK, after passing the peak moment of heat release. The reductions of chemical shrinkage induced by 10% and 20% MK are 28% and 36%, respectively, at the age of 7 days.

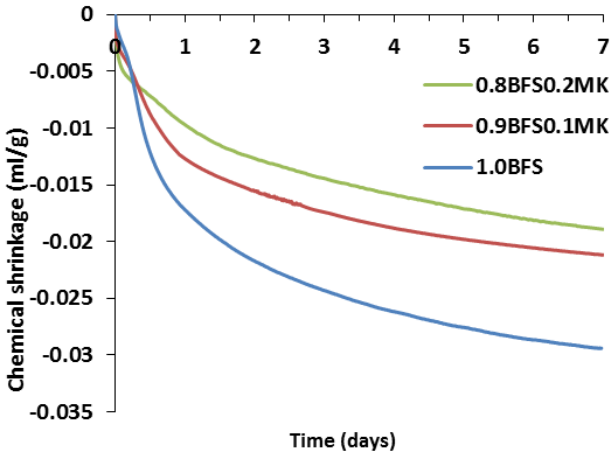

Fig. 8. Chemical shrinkage of AAS pastes with and without MK.

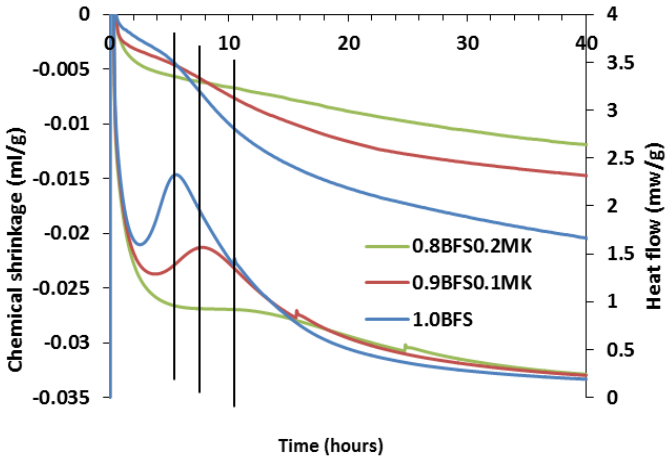

Fig. 9. Chemical shrinkage (shown in the primary axis) together with the heat evolution (shown in the secondary axis) of the pastes.

3.4 Internal RH and pore pressure

The measured internal RH and RH_S and the calculated RH_K and pore pressure at 1 day and 7 days are shown in Table 4.

The RH of the pore solutions of AAS pastes with and without MK are in the range of 70% - 80%, which are much lower than that of the pore solution in cement paste where a RH of above 95% was usually reported [67,68]. This is due to the high concentrations of Na^+ and OH^- in the pore solution of AAS as shown in Fig. 6. The RH_K values of the three mixtures decrease with elapse of time, indicating the self-desiccation process takes place in all mixtures.

By comparing the RH_K values of different pastes, it can be seen that the drop of internal RH due to the formation of menisci is mitigated by adding MK, and so is the pore pressure. 10% replacement of slag by MK results in a decrease in the pore pressure by 50% and 40% at day 1 and day 7, respectively. A higher amount of MK, i.e. 20%, decreases the pore pressure further, although the extent is less evident than that of the first 10% of MK.

Table 4

Internal RH and pore pressure within AAS pastes with and without MK.

	Specimens cured for 1 day				Specimens cured for 7 days			
Mixture	$RH(\%)$	$RH_S(\%)$	$RH_K(\%)$	σ(MPa)	$RH(\%)$	$RH_S(\%)$	$RH_K(\%)$	σ(MPa)
1.0BFS	71.6	73.9	96.8	4.4	65.9	74.1	89.0	15.8
0.9BFS0.1MK	76.7	77.9	98.4	2.2	73.9	78.9	93.6	8.95
0.8BFS0.2MK	79.1	80.2	98.6	1.9	77.6	82.0	94.5	7.61

3.5 Elastic modulus

The elastic modulus results are shown in Fig. 10. It can be seen that the elastic modulus of all the mixtures is above 14 GPa at the age of 1 day and experienced a slight increase during the following 6 days. The increment of the elastic modulus of 0.8BFS0.2MK is the most prominent,13%. Compared with the 1.0BFS mixture, the addition of 10% of MK improves slightly the elastic modulus at 1 day, while 20% of MK addition is beneficial to the elastic modulus only at 7 days. Nonetheless, the differences among the elastic modulus values for the three mixtures at the same age are smaller than 5%. This means that the addition of MK has minimal influence on the elastic modulus of the paste.

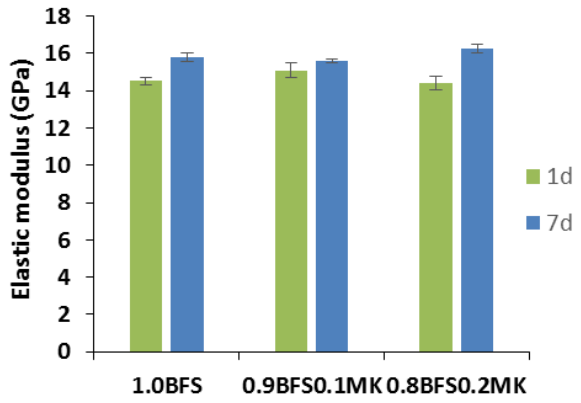

Fig. 10. Elastic modulus of AAS pastes with and without MK.

3.6 Compressive and flexural strength

As shown in Fig. 11 (a), the compressive strength of AAS decreases after the addition of MK. For example, the compressive strength at 7 days decreases by 8% and 20% when 10% and 20% of MK are added, respectively. Nonetheless, all mixture experienced large increments in compressive strength with elapse of time and the differences between different mixtures at 28 days are smaller than 21%.

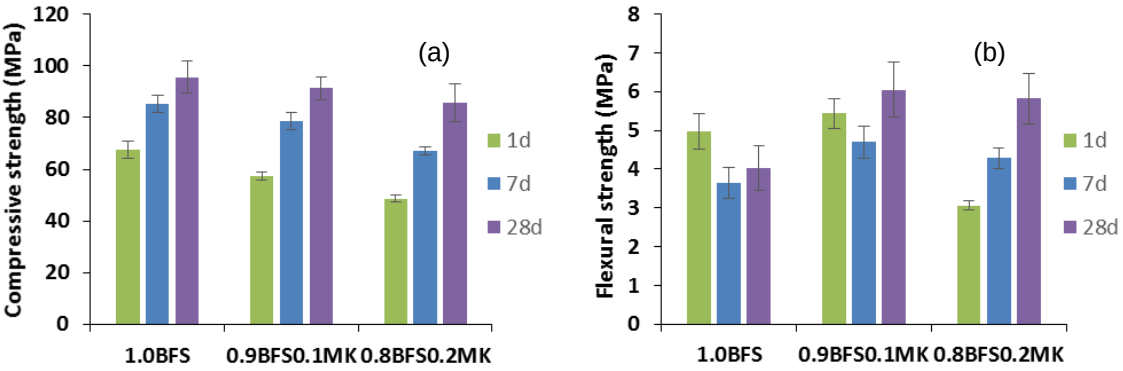

Fig. 11. (a) Compressive strength and (b) flexural strength of AAS pastes with and without MK.

Fig. 11 (b) shows that 0.8BFS0.2MK has the lowest flexural strength at 1 day, but it exceeds the flexural strength of 1.0BFS after 7 days. The flexural strength of 1.0BFS and 0.9BFS0.1MK decreases after one day and increase after curing for 7 days. Fig. 11 (b) also illustrates that the substitution of 10% and 20% slag by MK can improve the 7-day flexural strength of AAS paste by around 30% and 18%, respectively. At 28 days, the increments in flexural strength are further strengthened.

4. Discussion

4.1 Influence of MK on reaction products, reaction kinetics and pore structure

By combining the characterization results, a comprehensive understanding of the influence of MK addition on the reaction process and microstructure evolution of AAS paste can be obtained. This part would act as a basis for understanding the shrinkage mitigating effect of MK.

The XRD and FTIR results show that the major reaction products formed in the studied mixtures are CASH gels (Fig. 3 and Fig. 4). FTIR results indicate the existence of NASH gels in slag/MK blended systems at the age of 1 day (Fig. 4), but the signal disappears at 7 days. This is because the NASH gels are not stable in the presence of Ca at high alkalinity, and tend to gradually convert into CASH gels until a minimum Ca/Si, or a maximum Al/Si molar ratio is reached in the composition of CASH gels [37]. Due to the low content of MK in the mixture, it is unlikely to reach the minimum Ca/Si, or the maximum Al/Si ratio in the current composition of the reaction products. Therefore, the transformation of NASH gels to CASH gels takes place until all the NASH gels are consumed.

The XRD and FTIR results, together with the calorimetry results (Fig. 5) show that the formation of the primary binder phase is retarded when MK is incorporated into the system, and this effect can be explained through the pore solution composition results as shown in Fig. 6. It can be seen in Fig. 6 (a) that the concentrations of Na^+ and OH^- in the pore solution only slightly change with time in plain AAS paste. This is confirmed by the RH_S data of the 1.0BFS pore solution, which varies little from 1 day (73.9%) to 7 days (74.1%), since the RH_S is linearly related to the molar fraction of the water in the pore solution according to Raoult's law [69]. In slag/MK blended systems, in contrast, the concentration of Na^+ and OH^- is more significantly reduced with elapse of time (Fig. 6 (a)). This reduction is because of the dissolution of MK consumes Na^+ and OH^-, according to Davidovits [66]. The reduced OH^- is

detrimental to the dissolution of slag and formation of CASH gels as reported by Zuo et al. [70]. The retarded dissolution of slag is confirmed by the Ca concentration results shown in Fig. 6 (c). In the meantime, the dissolution of MK releases additional Si and Al to the system (Fig. 6 (b)), which would favor the formation of NASH gels or zeolite rather than the CASH gels when Ca is not largely available in the pore solution, as indicated by Bernal et al. [38] and Gharzouni et al. [71]. This explains the existence of a small amount of NASH gels in slag/MK blended systems at very early age. In fact, evidences of the retarding effect of extra Si and/or Al on the formation CASH gels can be found in many studies which investigated the reaction kinetics of AAS system modified by incorporation of fly ash or by activator with higher modulus (SiO_2/Na_2O) [65,72–75]. For example, Ismail et al. [75] reported that the incorporation of fly ash, as an additional source of Si and Al, but not Ca, into AAS system decreases the rate of formation of CASH gels (the main binding gels). A higher Al_2O_3 content in the precursor, i.e. slag, can also slow down the hydration of slag as reported by Ben Haha et al. [76]. These results corroborate the retarding effect of MK on the hydration of slag observed in this study.

Due to the delayed formation of the major reaction products, the pore refinement in the paste is also retarded when MK is present, as shown in Fig. 7. The final setting time is delayed by MK addition, as shown in Table 3. A similar effect of MK on the setting time of AAS was also found by Cheng and Chiu [77]. The prolonged setting time is beneficial to the application of AAS systems since they are known to harden more rapidly than usually desired [7].

It is worth noting that the influences of MK on the reaction process of AAS become less predominant at 7 days compared with 1 day. As indicated by Fig. 3 – Fig. 6, the reaction products, ions concentrations in the pore solution and the total heat releases of the three mixtures become more similar as the reactions going on. This is at odds with the results obtained by Bernal et al. [38] and Buchwald et al. [33], who found a clear difference between the long-term reaction products in plain AAS (CASH gels) and in BFS/MK blends (coexistence of CASH gels and NASH gels or zeolite). This discrepancy is actually due to two reasons. First, the MK content in this study is low. 10% - 20% of MK cannot dramatically change the final chemical compositions (e.g. Si/Al and Ca/Si) of the reaction products. Second, the curing temperature utilized in this study is 20 °C , while 27 °C and 40 °C were adopted in [38] and [33], respectively. The elevated temperature is favorable or even necessary for the formation of NASH gels or zeolites, especially when a large amount of Ca is present [37,78]. At ambient temperature, however, CASH gels are more stable in slag-based systems [79], as in the case of this study.

4.2 Influence of MK on autogenous shrinkage

By retarding the reaction process and pore structure development in AAS, the incorporation of MK mitigate the driving force of autogenous shrinkage. Since the hydration of slag and the formation of reaction products are delayed by MK addition, the chemical shrinkage of the paste is decreased as the content of MK increases, as shown in Fig. 8. Actually, the development of chemical shrinkage determines the potential of self-desiccation in cementitious materials and also in AAS systems [50]. Chemical shrinkage means that the absolute volume of reaction products is smaller than the total volume of reactants, which are cement and water for OPC and slag and activator for AAS. With the reaction going on, the absolute volume of the whole system keeps decreasing, and more internal voids are being

created and occupied by air or gas. As the liquid is consumed gradually from bigger pores to smaller pores, the curvature radius of the menisci between liquid and gas decreases and capillary pressure or pore pressure develops [80]. When MK is present in AAS, the chemical shrinkage is reduced (Fig. 8), so that less volume within the paste is occupied by gas or air; and meanwhile the pore structure becomes coarser (Fig. 7). These two factors determine that the radius of the menisci in the slag/MK blends at the same curing age would be smaller than in plain AAS paste, which means a smaller pore pressure. This has been confirmed by the internal RH_K data as shown in Table 4, where lower RH_K indicates larger menisci and lower pore pressure.

It needs to be pointed out that while the level of pore pressure indicates the driving force, the measured autogenous shrinkage also depends on the compressibility of the paste, in particular on the elastic modulus [50]. As shown in Fig. 10, the substitution of slag by MK does not induce much effect on the elastic modulus development of the paste (the reason will be discussed further in Section 4.4). As a result of the considerably reduced pore pressure and the rarely affected elastic modulus, the autogenous shrinkage of the MK-containing paste is largely mitigated.

4.3 Comparison between measured and calculated autogenous shrinkage

The autogenous shrinkage of AAS pastes can be calculated based on existing experimental results. According to Bentz et al. [81], the linear autogenous shrinkage of a paste can be simulated by Eq. (5):

$$\varepsilon_{lin} = \frac{S\sigma}{3}\left(\frac{1}{K} - \frac{1}{K_S}\right) \tag{5}$$

where S is the saturation degree of the paste, a ratio of liquid to the total volume of pores (-); σ is the pore pressure (MPa), see Table 4; K is the bulk modulus of the whole porous body (MPa) and K_S is the bulk modulus of the solid material (GPa). Strictly speaking, this equation can only give the linear elastic deformation and creep is not taken into account [49].

The saturation degree S can be calculated from the non-evaporable water content and chemical shrinkage, according to Eq. (6) [50]:

$$S = \frac{V_l}{V_p} = \frac{V_{il} - V_{nl}}{V_{il} - V_{nl} + V_{cs}} \tag{6}$$

where V_l (ml) is the liquid volume in the paste, V_p (ml) is the total pore volume in the paste, V_{il} (ml) is the initial liquid content, V_{nl} (ml) is the non-evaporable liquid volume, and V_{cs} (ml) is the volume of chemical shrinkage, see Fig. 8.

In Eq. (6) the initial air content of the paste is not considered. The non-evaporable water is determined by measuring the weight loss per gram of the sample between 105 °C and 950 °C. To obtain the volume of the non-evaporable liquid through the non-evaporable water content, it is assumed that the water proportion in the liquid and the density of the liquid are equal to those of the activator, which are 420 g water/590 g activator (see Table 2) and 1.31 g/ml (measured by pycnometer), respectively. The saturation degrees of the three mixtures in 1 day and 7 days are shown in Table 5.

Table 5

Saturation degree of AAS pastes with and without MK.

Mixture	**1.0BFS 1d**	**1.0BFS 7d**	**0.9BFS0.1MK 1d**	**0.9BFS0.1MK 7d**	**0.8BFS0.2MK 1d**	**0.8BFS0.2MK 7d**
S	0.952	0.913	0.964	0.938	0.974	0.946

The bulk modulus K of the paste is calculated using the following formula:

$$K = \frac{E}{3(1-2\upsilon)} \quad (7)$$

where E is elastic modulus (GPa) and υ is Poisson's ratio (–). The elastic modulus of the paste has been shown in Fig. 10. The Poisson's ratio of the pastes is assumed as 0.15 according to [82]. The K_S of the solid skeleton is assumed as 44 GPa according to [83]. The effect of the choice of K_S on the calculated shrinkage (Eq. 5) is only minor: a variation of K_S from 40 to 50 GPa leads to a 4% variation in the calculated shrinkage, as also indicated by Lura [50].

The calculated autogenous shrinkage of the pastes according to the equations above is shown in Fig. 12. It can be seen that the estimated autogenous shrinkages of the three mixtures at 7 days are around 530, 313 and 257 μ strain. Compared with the measured autogenous shrinkage shown in Fig.2, the calculated shrinkages at 7 days are 12.9, 13.5 and 13.7 times lower for the plain mixture, the mixtures containing 10% MK and 20% MK, respectively. These discrepancies are around 2 times as high as those reported for OPC pastes [84,85]. Zuo et al. [84] reported that the calculated autogenous shrinkage of OPC paste with water-to-cement ratio of 0.3 is about 5.5 times lower than the experimentally measured one. A similar discrepancy value, 4 times, was found by Sant et al. who also studied the OPC with 0.3 water-to-cement ratio [85].

The discrepancy between calculated and measured autogenous shrinkages for OPC was attributed by the authors of [84,85] to the viscoelastic response of OPC to the pore pressure, of which they only considered the elastic part in the calculation. The discrepancy found for AAS paste, which is 2 times as high as the one for OPC paste, may indicate that AAS exhibits more pronounced viscoelasticity than OPC. This point is consistent with the large non-elastic deformation and evident creep/relaxation reported for AAS paste and concrete [14,86–89]. According to Ye and Radlińska [14], the pronounced viscous characteristic of AAS is attributed to the rearrangement and reorganization of CASH gels under internal/external force. The reason why CASH gels are more viscoelastic compared with CSH gels probably lies in the structural incorporation of alkali cations in CASH, which reduces the stacking regularity of CASH layers and makes the gel easier to collapse and redistribute [14].

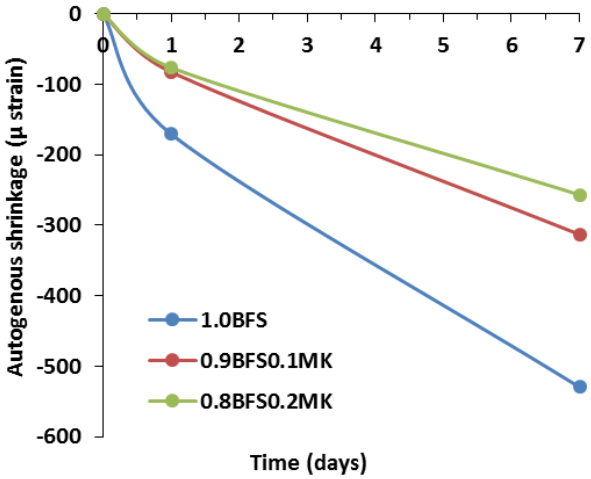

Fig. 12. Simulated autogenous shrinkage of AAS pastes with and without MK.

Although the amplitudes of the simulated autogenous shrinkage do not fit the measured data very well, it is worth noting that the calculated shrinkage curves show obvious gaps between the plain AAS mixture and the mixtures with MK. The reductions of the calculated autogenous shrinkage (i.e. the elastic deformation under pore pressure) at 7 days induced by 10% MK and 20% MK are 40% and 52%, respectively. These values are quite similar to the reductions of the total autogenous shrinkage, 38% and 50%, at this age (see Fig. 2). This indicates that the elastic shrinkage and the non-elastic shrinkage are mitigated proportionately with the incorporation of MK. If the viscoelasticity of AAS paste can be reduced, the autogenous shrinkage would also be mitigated. This strategy can be an interesting topic for future research. In addition, it should be noted that besides the pore pressure theory, other mechanisms may also exist for the autogenous shrinkage of AAS [90–92], which may be another reason for the misprediction of the deformation based on Eq. (5). Further research is required to figure out whether pore pressure resulting from self-desiccation is the exclusive driving force of autogenous shrinkage of AAS systems.

4.4 Influence of MK on mechanical properties

It is noticed that the influences of MK incorporation on the compressive strength, flexural strength and elastic modulus of AAS paste are different.

According to Fig. 11 (a), the compressive strength decreases with the increment of MK content. This is due to the formation of lower amounts of reaction products and coarser pore structure when MK is incorporated, as already presented above. In contrast, the flexural strength of the paste increases when 10% of MK is present. This increase can be explained by the mitigation effect of MK on microcracking development in AAS [93]. While compressive strength is mainly dependent on the porosity of the solid skeleton, the three-point bending flexural strength is much more sensitive to microcracking. Although the pastes are not under external restrained condition, the unreacted particles can act as local restraints to the autogenous shrinkage of the surrounding gels [94]. Since AAS without MK undergoes high autogenous shrinkage, microcracks may have developed within the paste, as also reported intensively in literature [93,95–97], and therefore harm the flexural strength of AAS paste [93,98]. When 10% MK is present, the autogenous shrinkage is greatly mitigated and so would be the development of microcracking, thus the flexural strength is improved. As for

0.8BFS0.2MK, the microcracks should be further mitigated, but its reaction degree at 1 day is too low, hence its flexural strength at 1 day is lower than 1.0BFS. Nonetheless, with the elapse of time, the flexural strength of 0.8BFS0.2MK still exceeds 1.0BFS. The development of microcracking due to autogenous shrinkage may also explain why the flexural strength of 1.0BFS and 0.9BFS0.1MK decreases from 1 day to 7 days.

Besides flexural strength, elastic modulus is also known to be sensitive to microcracking [99,100]. As shown in Fig. 10, three mixtures show similar elastic modulus at both 1 day and 7 days. This may be due to the coupled effects induced by MK addition: on one hand, AAS with MK has fewer reaction products and coarser pore structure which have a detrimental effect on the elastic modulus, but on the other hand the addition of MK mitigates the development of microcracking in the paste thus benefits the elastic modulus. As a result, the three mixtures exhibit similar elastic modulus values at 1 day and also 7 days.

It is worth noting that the improvement in flexural strength by MK is very beneficial to slag based alkali activated systems, which are reported to be strong in compression but relative weak under tensile stress [101,102]. This, besides the shrinkage mitigating effect, is another advantage of MK to be used as an admixture in AAS systems.

Considering the overall influences of MK addition on the autogenous shrinkage, microstructure and mechanical properties of AAS paste, it seems that 10% substitution of slag by MK shows optimal performances. Nonetheless, it should be noted that even the compressive strength of 0.8BFS0.2MK, 49 MPa at 1 day and 86 MPa at 28 days, are already adequate for most concrete mix design for practice. Therefore, 20% of MK can also be suitable for applications especially those require longer setting time and enhanced shrinkage-mitigation effect. Taking into account also the wide availability of MK as a low-cost product, there should be a promising potential in utilizing MK in slag-based alkali-activated concrete.

5. Conclusions

In this study, for the first time, the mitigating effect of MK on the autogenous shrinkage of AAS paste has been investigated. The knowledge and understanding of the mitigation mechanisms are obtained. The influences of MK addition on the mechanical properties of AAS are also discussed. Based on the presented results and discussion, the following conclusions can be drawn:

(1) The incorporation of MK leads to pronounced mitigation of the autogenous shrinkage of AAS. The reductions at 1 day are 44% and 60% by 10% and 20% substitutions of slag by MK, respectively.
(2) The addition of MK provides extra dissolvable Si and Al to the system and decreases the concentrations of Na^+ and OH^- in the pore solution. As a result, the hydration of slag and the formation of CASH gels are retarded. CASH gels are the major reaction products of the pastes, despite that some NASH type gels are formed in BFS/MK blends at very early age.
(3) The development of chemical shrinkage and the refinement of pore structure are hindered by addition of MK. The self-desiccation process and the pore pressure developed in the paste are considerably mitigated. Meanwhile, the elastic modulus is only slightly influenced when MK is incorporated. As a result, the autogenous shrinkage of AAS is effectively mitigated by MK.

(4) The compressive strength of AAS is slightly decreased by adding MK, while the flexural strength is greatly improved. 10% replacement of slag by MK leads to a larger increase of the flexural strength of AAS compared with 20% replacement.
(5) All the property improvements, such as reduced autogenous shrinkage, extended setting time and improved flexural strength with the incorporation of MK, suggest that MK is a very promising admixture to AAS systems. The dosages of MK studied in this work are of reference value for designing alkali-activated slag/MK blended materials.

Acknowledgment

This work is supported in part by the scholarship from China Scholarship Council (CSC) and the grant from Netherlands Organisation for Scientific Research (NWO).
Mr. Yibing Zuo at Microlab of Delft University of Technology is acknowledged for sharing the XRD data of slag. Ms. Yiru Yan at Empa is acknowledged for the discussion on the XRD and FTIR results. Prof. John Provis at University of Sheffield and Dr. Andreas Leemann at Empa are acknowledged for the discussion on elastic modulus and microcracking.

References

[1] H. Kühl, Slag cement and process of making the same, US Pat. 900 (1908) 939.

[2] A.O. Purdon, The action of alkalis on blast-furnace slag, J. Soc. Chem. Ind. 59 (1940) 191–202.

[3] D.M. Roy, Alkali-activated cements: Opportunities and challenges, Cem. Concr. Res. 29 (1999) 249–254. doi:10.1016/S0008-8846(98)00093-3.

[4] J.L. Provis, J.S.J. Van Deventer, Geopolymers: structures, processing, properties and industrial applications, Woodhead, Cambridge, UK, 2009.

[5] M.C.G. Juenger, F. Winnefeld, J.L. Provis, J.H. Ideker, Advances in alternative cementitious binders, Cem. Concr. Res. 41 (2011) 1232–1243. doi:10.1016/j.cemconres.2010.11.012.

[6] K. Arbi, M. Nedeljković, Y. Zuo, G. Ye, A Review on the Durability of Alkali-Activated Fly Ash/Slag Systems: Advances, Issues, and Perspectives, Ind. Eng. Chem. Res. 55 (2016) 5439–5453. doi:10.1021/acs.iecr.6b00559.

[7] S. Wang, X. Pu, K.L. Scrivener, P.L. Pratt, Alkali-activated slag cement and concrete: a review of properties and problems, Adv. Cem. Res. 7 (1995) 93–102. doi:10.1680/adcr.1995.7.27.93.

[8] A.M. Rashad, A comprehensive overview about the influence of different admixtures and additives on the properties of alkali-activated fly ash, Mater. Des. 53 (2014) 1005–1025. doi:10.1016/j.matdes.2013.07.074.

[9] A.A. Melo Neto, M.A. Cincotto, W. Repette, Drying and autogenous shrinkage of pastes and mortars with activated slag cement, Cem. Concr. Res. 38 (2008) 565–574. doi:10.1016/j.cemconres.2007.11.002.

[10] M. Palacios, F. Puertas, Effect of superplastisizer and shrinkage reducing admixtures on alkali-activated slag pastes and mortars, Cem. Concr. Res. 35 (2005) 1358–1367. doi:10.1016/j.cemconres.2004.10.014.

[11] C. Cartwright, F. Rajabipour, A. Radli, Shrinkage Characteristics of Alkali-Activated Slag Cements, J. Mater. Civ. Eng. 27 (2014) 1–9. doi:10.1061/(ASCE)MT.1943-5533.0001058.

[12] M. Palacios, F. Puertas, Effect of shrinkage-reducing admixtures on the properties of alkali-activated slag mortars and pastes, Cem. Concr. Res. 37 (2007) 691–702.

[13] A.R. Sakulich, D.P. Bentz, Mitigation of autogenous shrinkage in alkali activated slag mortars by internal curing, Mater. Struct. 46 (2013) 1355–1367. doi:10.1617/s11527-012-9978-z.

[14] H. Ye, A. Radlińska, Shrinkage mechanisms of alkali-activated slag, Cem. Concr. Res. 88 (2016) 126–135. doi:10.1016/j.cemconres.2016.07.001.

[15] H. Ye, A. Radlińska, Shrinkage mitigation strategies in alkali-activated slag, Cem. Concr. Res. 101 (2017) 131–143. doi:10.1016/j.cemconres.2017.08.025.

[16] Z. Li, M. Nedeljkovic, Y. Zuo, G. Ye, Autogenous shrinkage of alkali-activated slag-fly ash pastes, in: 5th Int. Slag Valoris. Symp., Leuven, 2017: pp. 369–372.

[17] F. Collins, J.. Sanjayan, Effect of pore size distribution on drying shrinking of alkali-activated slag concrete, Cem. Concr. Res. 30 (2000) 1401–1406. doi:10.1016/S0008-8846(00)00327-6.

[18] F. Collins, J.G. Sanjayan, Microcracking and strength development of alkali activated slag concrete, Cem. Concr. Compos. 23 (2001) 345–352. doi:10.1016/S0958-9465(01)00003-8.

[19] N.K. Lee, J.G. Jang, H.K. Lee, Shrinkage characteristics of alkali-activated fly ash/slag paste and mortar at early ages, Cem. Concr. Compos. 53 (2014) 239–248. doi:10.1016/j.cemconcomp.2014.07.007.

[20] H. Ye, Creep Mechanisms of Calcium-Silicate-Hydrate: An Overview of Recent Advances and Challenges, Int. J. Concr. Struct. Mater. 9 (2015) 453–462. doi:10.1007/s40069-015-0114-7.

[21] B.D. Kumarappa, S. Peethamparan, M. Ngami, Autogenous shrinkage of alkali activated slag mortars: Basic mechanisms and mitigation methods, Cem. Concr. Res. 109 (2018) 1–9. doi:10.1016/j.cemconres.2018.04.004.

[22] S. Oh, Y.C. Choi, Superabsorbent polymers as internal curing agents in alkali activated slag mortars, Constr. Build. Mater. 159 (2018) 1–8. doi:10.1016/j.conbuildmat.2017.10.121.

[23] C. Song, Y.C. Choi, S. Choi, Effect of internal curing by superabsorbent polymers – Internal relative humidity and autogenous shrinkage of alkali-activated slag mortars, Constr. Build. Mater. 123 (2016) 198–206. doi:10.1016/j.conbuildmat.2016.07.007.

[24] M. Criado, A. Palomo, A. Fernández-Jiménez, P.F.G. Banfill, Alkali activated fly ash: Effect of admixtures on paste rheology, Rheol. Acta. 48 (2009) 447–455. doi:10.1007/s00397-008-0345-5.

[25] G. Habert, J.B. D'Espinose De Lacaillerie, N. Roussel, An environmental evaluation of geopolymer based concrete production: Reviewing current research trends, J. Clean. Prod. 19 (2011) 1229–1238. doi:10.1016/j.jclepro.2011.03.012.

[26] C.A. Rees, J.L. Provis, G.C. Lukey, J.S.J. van Deventer, The mechanism of geopolymer gel formation investigated through seeded nucleation, Colloids Surfaces A Physicochem. Eng. Asp. 318 (2008) 97–105. doi:10.1016/j.colsurfa.2007.12.019.

[27] T. Bakharev, J.G. Sanjayan, Y. Cheng, Effect of elevated temperature curing on properties of alkali-activated slag concrete, Cem. Concr. Res. 29 (1999) 1619–1625.

[28] T. Bakharev, J.. Sanjayan, Y. Cheng, Alkali activation of Australian slag cements, Cem. Concr. Res. 29 (1999) 113–120. doi:10.1016/S0008-8846(98)00170-7.

[29] W. Shen, Y. Wang, T. Zhang, M. Zhou, J. Li, X. Cui, Magnesia modification of alkali-activated slag fly ash cement, J. Wuhan Univ. Technol. Mater. Sci. Ed. 26 (2011) 121–125. doi:10.1007/s11595-011-0182-8.

[30] M. Chi, R. Huang, Binding mechanism and properties of alkali-activated fly ash/slag mortars, Constr. Build. Mater. 40 (2013) 291–298. doi:10.1016/j.conbuildmat.2012.11.003.

[31] Z. Hu, Early hydration and shrinkage of alkali-activated slag/fly ash blend cement, Hunan University, 2013.

[32] C.K. Yip, G.C. Lukey, J.S.J. Van Deventer, The coexistence of geopolymeric gel and calcium silicate hydrate at the early stage of alkaline activation, Cem. Concr. Res. 35 (2005) 1688–1697. doi:10.1016/j.cemconres.2004.10.042.

[33] A. Buchwald, H. Hilbig, C. Kaps, Alkali-activated metakaolin-slag blends - Performance and structure in dependence of their composition, J. Mater. Sci. 42 (2007) 3024–3032. doi:10.1007/s10853-006-0525-6.

[34] S.A. Bernal, E.D. Rodrı´guez, R. Mejı´a De Gutie´rrez, M. Gordillo, J.L. Provis, Mechanical and thermal characterisation of geopolymers based on silicate-activated metakaolin/slag blends, J. Mater. Sci. 46 (2011) 5477–5486. doi:10.1007/s10853-011-5490-z.

[35] A. Buchwald, R. Tatarin, D. Stephan, Reaction progress of alkaline-activated metakaolin-ground granulated blast furnace slag blends, J. Mater. Sci. 44 (2009) 5609–5617. doi:10.1007/s10853-009-3790-3.

[36] S.A. Bernal, J.L. Provis, V. Rose, R.M. De Gutiérrez, High-resolution X-ray diffraction and fluorescence microscopy characterization of alkali-activated slag-metakaolin binders, J. Am. Ceram. Soc. 96 (2013) 1951–1957. doi:10.1111/jace.12247.

[37] I. Garcia-Lodeiro, A. Palomo, A. Fernández-Jiménez, D.E. MacPhee, Compatibility studies between N-A-S-H and C-A-S-H gels. Study in the ternary diagram Na2O-CaO-Al2O3-SiO 2-H2O, Cem. Concr. Res. 41 (2011) 923–931. doi:10.1016/j.cemconres.2011.05.006.

[38] S.A. Bernal, J.L. Provis, V. Rose, R. Mejía De Gutierrez, Evolution of binder structure in sodium silicate-activated slag-metakaolin blends, Cem. Concr. Compos. 33 (2011) 46–54. doi:10.1016/j.cemconcomp.2010.09.004.

[39] S.A. Bernal, R. Mejía De Gutiérrez, J.L. Provis, Engineering and durability properties of

concretes based on alkali-activated granulated blast furnace slag/metakaolin blends, Constr. Build. Mater. 33 (2012) 99–108. doi:10.1016/j.conbuildmat.2012.01.017.

[40] Z. Shi, C. Shi, J. Zhang, S. Wan, Z. Zhang, Z. Ou, Alkali-silica reaction in waterglass-activated slag mortars incorporating fly ash and metakaolin, Cem. Concr. Res. 108 (2018) 10–19. doi:10.1016/j.cemconres.2018.03.002.

[41] S.A. Bernal, R.M. de Gutierrez, J.L. Provis, V. Rose, Effect of silicate modulus and metakaolin incorporation on the carbonation of alkali silicate-activated slags, Cem. Concr. Res. 40 (2010) 898–907. doi:10.1016/j.cemconres.2010.02.003.

[42] O. Burciaga-Díaz, R.X. Magallanes-Rivera, J.I. Escalante-Garcia, Alkali-activated slag-metakaolin pastes: Strength, structural, and microstructural characterization, J. Sustain. Cem. Mater. 2 (2013) 111–127. doi:10.1080/21650373.2013.801799.

[43] ASTM C1968, Standard Test Method for Autogenous Strain of Cement Paste and Mortar, (2013) 1–8. doi:10.1520/C1698-09.2.

[44] ASTM C191, Standard Test Methods for Time of Setting of Hydraulic Cement by Vicat Needle BT - Standard Test Methods for Time of Setting of Hydraulic Cement by Vicat Needle, (2013).

[45] M. Nedeljkovic, K. Arbi, Y. Zuo, G. Ye, Physical properties and pore solution ananlysis of alkali activated fly ash-slag pastes, Int. RILEM Conf. Mater. Syst. Struct. Civ. Eng. Conf. Segm. Concr. with Suppl. Cem. Mater. (2016).

[46] E.P. Barrett, L.G. Joyner, P.P. Halenda, The determination of pore volume and area distributions in porous substances. I. Computations from nitrogen isotherms, J. Am. Chem. Soc. 73 (1951) 373–380.

[47] Z. Li, S. Zhang, Y. Zuo, W. Chen, G. Ye, Chemical deformation of metakaolin based geopolymer, Cem. Concr. Res. 120 (2019) 108–118. doi:10.1016/j.cemconres.2019.03.017.

[48] H. Huang, G. Ye, Examining the “time-zero” of autogenous shrinkage in high/ultra-high performance cement pastes, Cem. Concr. Res. 97 (2015) 107–114. doi:10.1016/j.cemconres.2017.03.010.

[49] P. Lura, O.M. Jensen, K. Van Breugel, Autogenous shrinkage in high-performance cement paste: An evaluation of basic mechanisms, Cem. Concr. Res. 33 (2003) 223–232. doi:10.1016/S0008-8846(02)00890-6.

[50] P. Lura, Autogenous Deformation and Internal Curing of Concrete, Delft University of Technology, 2003.

[51] B. Delsaute, C. Boulay, J. Granja, J. Carette, M. Azenha, C. Dumoulin, G. Karaiskos, A. Deraemaeker, S. Staquet, Testing Concrete E-modulus at Very Early Ages Through Several Techniques: An Inter-laboratory Comparison, Strain. (2016) 91–109. doi:10.1111/str.12172.

[52] NEN 196-1, Methods of Testing Cement–Part 1: Determination of Strength, , 2005., Eur. Comm. Stand. (2005).

[53] E. ichi Tazawa, S. Miyazawa, T. Kasai, Chemical shrinkage and autogenous shrinkage of hydrating cement paste, Cem. Concr. Res. 25 (1995) 288–292. doi:10.1016/0008-8846(95)00011-9.

[54] E. ichi Tazawa, S. Miyazawa, Influence of cement and admixture on autogenous shrinkage of cement paste, Cem. Concr. Res. 25 (1995) 281–287. doi:10.1016/0008-8846(95)00010-0.

[55] M. Ben Haha, G. Le Saout, F. Winnefeld, B. Lothenbach, Influence of activator type on hydration kinetics, hydrate assemblage and microstructural development of alkali activated blast-furnace slags, Cem. Concr. Res. 41 (2011) 301–310. doi:10.1016/j.cemconres.2010.11.016.

[56] I. García Lodeiro, A. Fernández-Jimenez, A. Palomo, D.E. Macphee, Effect on fresh C-S-H gels of the simultaneous addition of alkali and aluminium, Cem. Concr. Res. 40 (2010) 27–32. doi:10.1016/j.cemconres.2009.08.004.

[57] I. García-Lodeiro, A. Fernández-Jiménez, M.T. Blanco, A. Palomo, FTIR study of the sol-gel synthesis of cementitious gels: C-S-H and N-A-S-H, J. Sol-Gel Sci. Technol. 45 (2008) 63–72. doi:10.1007/s10971-007-1643-6.

[58] M. Zhang, M. Zhao, G. Zhang, T. El-Korchi, M. Tao, A multiscale investigation of reaction kinetics, phase formation, and mechanical properties of metakaolin geopolymers, Cem. Concr. Compos. 78 (2017) 21–32. doi:10.1016/j.cemconcomp.2016.12.010.

[59] A. Fernández-Jiménez, A. Palomo, Alkali activated fly ashes. Structural studies through mid-infrared spectroscopy, Microporous Mesoporous Mat. 86 (2005) 207–214.

[60] W. Nocuń-Wczelik, Heat evolution in alkali activated synthetic slag--metakaolin mixtures, J. Therm. Anal. Calorim. 86 (2006) 739–743.

[61] C. Shi, R.L. Day, A calorimetric study of early hydration of alkali-slag cements, Cem. Concr. Res. 25 (1995) 1333–1346.

[62] A. Fernández-Jiménez, F. Puertas, Alkali-activated slag cements: kinetic studies, Cem. Concr. Res. 27 (1997) 359–368.

[63] A. Fernandez-Jimenez, F. Puertas, A. Arteaga, Determination of kinetic equations of alkaline activation of blast furnace slag by means of calorimetric data, J. Therm. Anal. Calorim. 52 (1998) 945–955.

[64] A.M. Neville, Properties of Concrete, 2011.

[65] D. Krizan, B. Zivanovic, Effects of dosage and modulus of water glass on early hydration of alkali-slag cements, Cem. Concr. Res. 32 (2002) 1181–1188. doi:10.1016/S0008-8846(01)00717-7.

[66] J. Davidovits, Geopolymer Chemistry & Applications, 4 th, Institut Géopolymère, Saint-Quentin, France, 2015.

[67] H. Chen, M. Wyrzykowski, K. Scrivener, P. Lura, Prediction of self-desiccation in low water-to-cement ratio pastes based on pore structure evolution, Cem. Concr. Res. 49 (2013) 38–47. doi:10.1016/j.cemconres.2013.03.013.

[68] M. Nedeljković, B. Ghiassi, S. van der Laan, Z. Li, G. Ye, Effect of curing conditions on the pore solution and carbonation resistance of alkali-activated fly ash and slag pastes, Cem. Concr. Res. J. 116 (2019) 146–158. doi:10.1016/j.conbuildmat.2017.12.005.

[69] O.M. Jensen, Autogenous deformation and RH-change—self-desiccation and self-desiccation shrinkage (in Danish), Phd Thesis, Build. Mater. Lab. Tech. Univ. Denmark, Lyngby, Denmark. 285 (1993).

[70] Y. Zuo, M. Nedeljković, G. Ye, Coupled thermodynamic modelling and experimental study of sodium hydroxide activated slag, Constr. Build. Mater. 188 (2018) 262–279.

[71] A. Gharzouni, L. Ouamara, I. Sobrados, S. Rossignol, Alkali-activated materials from different aluminosilicate sources: Effect of aluminum and calcium availability, J. Non. Cryst. Solids. 484 (2018) 14–25. doi:10.1016/j.jnoncrysol.2018.01.014.

[72] X. Gao, Q.L. Yu, H.J.H. Brouwers, Reaction kinetics, gel character and strength of ambient temperature cured alkali activated slag-fly ash blends, Constr. Build. Mater. 80 (2015) 105–115. doi:10.1016/j.conbuildmat.2015.01.065.

[73] N.K. Lee, H.K. Lee, Reactivity and reaction products of alkali-activated, fly ash/slag paste, Constr. Build. Mater. 81 (2015) 303–312. doi:10.1016/j.conbuildmat.2015.02.022.

[74] D. Ravikumar, N. Neithalath, Reaction kinetics in sodium silicate powder and liquid activated slag binders evaluated using isothermal calorimetry, Thermochim. Acta. 546 (2012) 32–43. doi:10.1016/j.tca.2012.07.010.

[75] I. Ismail, S.A. Bernal, J.L. Provis, R. San Nicolas, S. Hamdan, J.S.J. Van Deventer, Modification of phase evolution in alkali-activated blast furnace slag by the incorporation of fly ash, Cem. Concr. Compos. 45 (2014) 125–135. doi:10.1016/j.cemconcomp.2013.09.006.

[76] M. Ben Haha, B. Lothenbach, G. Le Saout, F. Winnefeld, Influence of slag chemistry on the hydration of alkali-activated blast-furnace slag - Part II: Effect of Al2O3, Cem. Concr. Res. 42 (2012) 74–83. doi:10.1016/j.cemconres.2011.08.005.

[77] T.-W. Cheng, J.P. Chiu, Fire-resistant geopolymer produced by granulated blast furnace slag, Miner. Eng. 16 (2003) 205–210.

[78] Y. Ma, Microstructure and Engineering Properties of Alkali Activated Fly Ash -as an environment friendly alternative to Portland cement, 2013.

[79] J.L. Provis, Alkali-activated materials, Cem. Concr. Res. 114 (2018) 40–48. doi:10.1016/j.cemconres.2017.02.009.

[80] O.M. Jensen, P.F. Hansen, Autogenous deformation and RH-change in perspective, Cem. Concr. Res. 31 (2001) 1859–1865. doi:10.1016/S0008-8846(01)00501-4.

[81] D.P. Bentz, E.J. Garboczi, D.A. Quenard, Modelling drying shrinkage in reconstructed porous materials: application to porous Vycor glass, Model. Simul. Mater. Sci. Eng. 6 (1998) 211.

[82] S. Prinsse, Alkali-activated concrete: development of material properties (strength and stiffness) and flexural behaviour of reinforced beams over time, Master Thesis. (2017).

[83] L.F. Nielsen, A research note on sorption, pore size distribution, and shrinkage of porous materials, Danmarks Tekniske Højskole. Laboratoriet for Bygningsmaterialer, 1991.

[84] W. Zuo, P. Feng, P. Zhong, Q. Tian, N. Gao, Y. Wang, C. Yu, C. Miao, Effects of novel polymer-type shrinkage-reducing admixture on early age autogenous deformation of cement pastes, Cem. Concr. Res. 100 (2017) 413–422. doi:10.1016/j.cemconres.2017.08.007.

[85] G. Sant, B. Lothenbach, P. Juilland, G. Le Saout, J. Weiss, K. Scrivener, The origin of early age expansions induced in cementitious materials containing shrinkage reducing admixtures, Cem. Concr. Res. 41 (2011) 218–229.

[86] Z. Li, A. Kostiuchenko, G. Ye, Autogenous shrinkage-induced stress of alkali-activated slag and fly ash concrete under restraint condition, in: ECI (Ed.), Alkali Act. Mater. Geopolymers Versatile Mater. Offer. High Perform. Low Emiss., Tomar, 2018: p. 24.

[87] H. Ye, C. Cartwright, F. Rajabipour, A. Radlińska, Understanding the drying shrinkage performance of alkali-activated slag mortars, Cem. Concr. Compos. 76 (2017) 13–24. doi:10.1016/j.cemconcomp.2016.11.010.

[88] Z. Li, J. Liu, G. Ye, Drying shrinkage of alkali-activated slag and fly ash concrete. A comparative study with ordinary Portland cement concrete, in: Proc. Work. Concr. Model. Mater. Behav. Honor Profr. Klaas van Breugel, Delft, 2018: pp. 160–166.

[89] A. Kostiuchenko, J. Liu, Z. Aldin, Mechanical properties and creep behaivor of an alkali-activated concretemechanical properties and creep behaivor of an alkali-activated concrete, in: Alkali Act. Mater. Geopolymers Versatile Mater. Offer. High Perform. Low Emiss., 2018: p. 9.

[90] S. Uppalapati, O. Cizer, Understanding the autogenous shrinkage in alkali-activated slag/fly-ash blends, in: Int. Conf. ALKALI Act. Mater. GEOPOLYMERS VERSATILE Mater. Offer. HIGH Perform. LOW Emiss., 2018: p. 27.

[91] G. Fang, H. Bahrami, M. Zhang, Mechanisms of autogenous shrinkage of alkali-activated fly ash-slag pastes cured at ambient temperature within 24 h, Constr. Build. Mater. 171 (2018) 377–387. doi:10.1016/j.conbuildmat.2018.03.155.

[92] W. Tu, Y. Zhu, G. Fang, X. Wang, M. Zhang, Internal curing of alkali-activated fly ash-slag pastes using superabsorbent polymer, Cem. Concr. Res. 116 (2019) 179–190. doi:10.1016/j.cemconres.2018.11.018.

[93] M. Nedeljković, Z. Li, G. Ye, Setting, Strength, and Autogenous Shrinkage of Alkali-Activated Fly Ash and Slag Pastes: Effect of Slag Content, Materials (Basel). 11 (2018) 2121. doi:10.3390/ma11112121.

[94] P. Lura, O.M. Jensen, J. Weiss, Cracking in cement paste induced by autogenous shrinkage, Mater. Struct. Constr. 42 (2009) 1089–1099. doi:10.1617/s11527-008-9445-z.

[95] J.J. Thomas, A.J. Allen, H.M. Jennings, Density and water content of nanoscale solid C-S-H formed in alkali-activated slag (AAS) paste and implications for chemical shrinkage, Cem. Concr. Res. 42 (2012) 377–383. doi:10.1016/j.cemconres.2011.11.003.

[96] F. Collins, J.G. Sanjayan, cracking tendency of alkali-activated slag concrete subjected to restrained shrinkage, Cem. Concr. Res. 30 (2000) 791–798. doi:10.1016/S0008-8846(00)00243-X.

[97] M.H. Hubler, J.J. Thomas, H.M. Jennings, Influence of nucleation seeding on the hydration kinetics and compressive strength of alkali activated slag paste, Cem. Concr. Res. 41 (2011) 842–846.

[98] A. Wardhono, C. Gunasekara, D.W. Law, S. Setunge, Comparison of long term performance between alkali activated slag and fly ash geopolymer concretes, Constr. Build. Mater. 143 (2017) 272–279.

[99] R. Loser, A. Leemann, An accelerated sulfate resistance test for concrete, Mater. Struct. 49 (2016) 3445–3457.

[100] F.C.S. Carvalho, C.-N. Chen, J.F. Labuz, Measurements of effective elastic modulus and microcrack density, Int. J. Rock Mech. Min. Sci. 34 (1997) 43--e1.

[101] C. Duran Atiş, C. Bilim, Ö. Çelik, O. Karahan, Influence of activator on the strength and drying shrinkage of alkali-activated slag mortar, Constr. Build. Mater. 23 (2009) 548–555. doi:10.1016/j.conbuildmat.2007.10.011.

[102] G. Fang, W.K. Ho, W. Tu, M. Zhang, Workability and mechanical properties of alkali-activated fly ash-slag concrete cured at ambient temperature, Constr. Build. Mater. 172 (2018) 476–487.